Development of a Seedless Floating Growth Process in Solution for Synthesis of Crystalline ZnO Micro/Nanowire Arrays on Graphene: Towards High-Performance Nanohybrid Ultraviolet Photodetectors

Jianwei Liu, Rongtao Lu, Guowei Xu, Judy Wu,* Prem Thapa, and David Moore*

A seedless solution process is developed for controllable growth of crystalline ZnO micro/nanowire arrays directly on single-layer graphene sheets made in chemical vapor deposition (CVD). In particular, the alignment of the ZnO micro/nanowires correlates well with the density of the wires, which is determined by both the sample configuration in solution and the graphene surface cleaning. With increasing wire density, the ZnO micro/nanowire array alignment may be varied from horizontal to vertical by increasing the physical confinement. Ultraviolet photodetectors based on the vertically aligned ZnO micro/nanowires on graphene show high responsivity of 1.62 A W^{-1} per volt, a 500% improvement over epitxial ZnO sensors, a 300% improvement over ZnO nanoparticle sensors, and a 40% improvement over the previous best results for nanowire/graphene hybrid sensors. This seedless, floating growth process could be scaled up for large scale growth of oriented ZnO micro/nanowires on graphene at low costs.

1. Introduction

Graphene, a one-atom-thick planar sheet of sp^2 bonded carbon atoms, holds great promise for optoelectronic applications due to its high carrier mobility at room temperature in excess of 15 000 cm^2 V^{-1} s^{-1}, its optical transmittance of ≈97.9% to white light, its flexibility, and its light weight.[1–3] However, the zero band gap of graphene has presented a major hurdle to electronic and optoelectronic applications. While small sub-eV band gaps have been obtained in graphene nanoribbons or graphene nanomeshes,[4–6] it is often at the cost of significantly reduced mobility caused by charge fluctuations from various defects, primarily the uncontrolled nanoribbon edges. Recently, considerable efforts have been made to attach photosensitive materials to graphene to form hybrid structures with selected ranges of photoabsorption.[7] For example, a TiO_2/GO hybrid was synthesized using hydrolysis in combination with hydrothermal treatment as a photocatalyst for photodegradation of rhodamine B molecules.[8] Also, CdSe/ZnS core/shell nanocrystals were spin-coated onto exfoliated graphene flakes producing efficient energy transfer from the photoexcited CdSe/ZnS nanocrystals to graphene with a fluorescence intensity quenched by a factor of 70.[9] The ZnO/graphene hybrid is of particular interest because it combines the superior wavelength selectivity of ZnO and the charge mobility of graphene, both of which are critical to applications of ultraviolet (UV) photodetectors,[10] electron emitters,[11] and many other optoelectronic devices.[12,13] Interesting progress has been made in the fabrication of ZnO/graphene hybrids including chemical vapor deposition (CVD) of ZnO nanowires and nanowalls on CVD graphene,[14] and solution synthesis of ZnO nanorods on a variety of substrates including graphene flakes casted on to silicon or glass[10] and on CVD graphene transferred on to glass or polyethylene naphthalate.[15] The solution method[10,15] has a unique advantage in large-scale synthesis of hybrid ZnO/graphene nanostructures at low temperatures and low costs. This is in contrast to the high temperatures range of 450 °C to 900 °C for the CVD growth of ZnO nanostructures on graphene, which prevents use of many technologically important substrates such as glass and plastics.[14,16] In addition, the high ZnO growth temperature may lead to the formation of defects on graphene and hence degrade the charge mobility in graphene and the interface between graphene and ZnO, which are both crucial to optoelectronic applications. The reported solution method,[10,15] however, requires a ZnO seeding layer to initiate nucleation of ZnO on graphene. For example, ZnO quantum dots (QDs)[10] were mixed with graphene flakes to serve as seeds for the solution growth of ZnO nanorods with random orientations. To improve the graphene and ZnO interface, polycrystalline 200 nm thick ZnO seeding layers were generated using vacuum-based metal-organic

Dr. J. W. Liu, Dr. R. T. Lu, G. W. Xu, Prof. J. Z. Wu
Department of Physics and Astronomy
University of Kansas
Lawrence, KS 66045, USA
E-mail: liuw@ku.edu; jwu@ku.edu
Dr. P. Thapa, Dr. D. Moore
Microscopy & Analytical Imaging Laboratory
University of Kansas
Lawrence, KS 66045, USA

DOI: 10.1002/adfm.201300468

chemical vapor deposition (MOCVD) at 170–180 °C.[17] The ZnO seeding layer may also be formed chemically[15] via spin-coating of zinc acetate dehydrate in an ethanol solution on multilayer graphene followed by annealing at 100 °C. It should be noted that the generation of the ZnO seeding layer involves additional fabrication steps, and achieving surface uniformity of the seeding layer on large area graphene remains a hurdle. Furthermore, the fabrication of seeding layers involves exposing graphene to gases and chemicals at elevated temperatures which may introduce additional defects to graphene. This may be particularly detrimental for monolayer graphene which is preferred for optical and optoelectronic applications to maintain high electrical conductivity and optical transmittance.[15]

This work reports a novel, seedless, floating growth scheme for the synthesis of ZnO micro/nanowires on CVD graphene sheets in solution (see **Figure 1**). Crystalline ZnO micro/nanowire arrays, aligned predominantly along the normal direction to the graphene, were obtained at low growth temperatures around 80 °C. It has been found that the alignment of the ZnO micro/nanowires correlates well with the physical confinement depending on the nucleation density of the wires. The ZnO micro/nanowire arrays' alignment was controlled by the physical confinement; increasing this confinement changed the alignment from horizontal (parallel to graphene) to vertical (perpendicular to graphene). This work represents the first success in low-cost fabrication of aligned ZnO micro/nanowire arrays directly on CVD graphene sheets without any seeding layer, and the process can be readily scaled up for industrial applications. Eliminating the seeding layer is important not only to simplify the ZnO/graphene nanohybrid fabrication process, but also to minimize damage to single-layer graphene to maintain its high electrical conductivity and optical transmittance. UV photodetectors have been fabricated using these ZnO/graphene nanohybrids, and high photoresponses and fast response times have been demonstrated. In this paper, we report our experimental results.

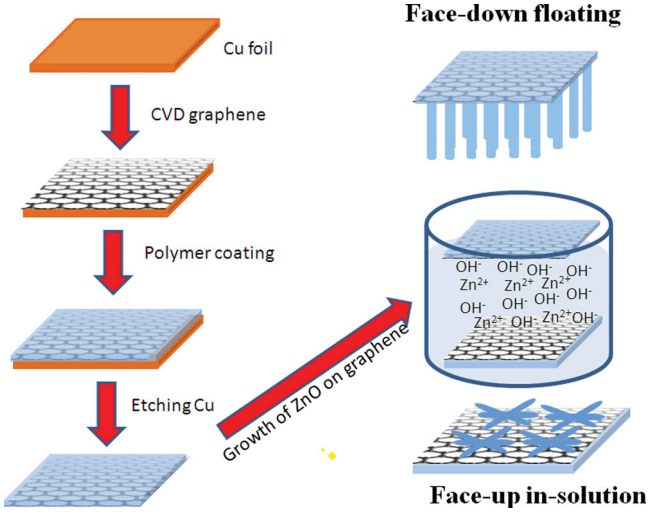

Figure 1. Schematic of the seedless face-up in solution and face-down floating growth of ZnO micro/nanowires on graphene films. The graphene sheet is supported by PMMA (transparent blue) and placed face-down or face-up (transferred on glass or silicon substrates) during the ZnO growth in solution.

2. Results and Discussion

Figure 1 schematically depicts the seedless floating growth process with CVD graphene sheets supported by a thin layer of polymer such as poly-methyl methacrylate (PMMA). Since the polymer/graphene sample has a lower density than that of the solution, it floats on the surface of the solution with the graphene side facing down. For a comparison, a face-up configuration was also examined (Figure 1) with graphene transferred on Si (or glass) substrates. In this case, the samples remained at the bottom of the solution with the graphene side facing up. It has been found that the difference in the growth configurations affects the ZnO nucleation and evolution dramatically. In particular, the accumulation of residues on the graphene can be minimized in the face-down configuration. This is critical to the nucleation of ZnO crystallites directly on CVD graphene, on which various growth defects[18] may serve as nucleation sites for the hydroxyl groups (-OH) to attach.[19] The growth process of ZnO in solution is divided into two steps: diffusion of the reactants to the nucleation sites on the graphene surface followed by reaction at the surface.[20] In an aqueous solution, $Zn(NO_3)_2$ decomposes into Zn cations (Zn^{2+}) and NO_3 anions (NO_3^{-1}). The Zn cation reacts with $NH_3.H_2O$ to form $Zn(NH_3)_4^{2+}$. Since CVD graphene contains a large number of defects, the hydroxyl groups (-OH) from the solution can easily attach to the defects of graphene and reacted with $Zn(NH_3)_4^{2+}$ to form $Zn(OH)_4^{2-}$ releasing ammonia, since the stability constant[21] of $Zn(OH)_4^{2-}$ ($lg\beta_4 = 17.66$) is higher than that of $Zn(NH_3)_4^{2+}$ ($lg\beta_4 = 9.46$). $Zn(OH)_4^{2-}$ decomposed and led to nucleation and growth of ZnO on graphene via the following reaction:

$$NH_3.H_2O \leftrightarrow NH_4^+ + OH^-$$
$$NH_3.H_2O \leftrightarrow NH_3 + H_2O$$
$$Zn^{2+} + 4NH_3 \leftrightarrow Zn(NH_3)_4^{2+} + 4OH^- \leftrightarrow Zn(OH)_4^{2-} + 4NH_3$$
$$Zn(OH)_4^{2-} \leftrightarrow ZnO + H_2O + 2OH^-$$

Ammonium hydroxide in the growth process not only provides OH^-, but also reacts with zinc ions to form a complex, which can kinetically control the species in the solution and keep the free zinc ion concentration low.

Since the surface condition of the CVD graphene can sensitively affect the initial nucleation stage, two groups of samples were compared in the face-down configuration with different cleaning treatments of the CVD graphene surfaces prior to ZnO growth. In one group (Group A), the graphene film was treated with a standard transfer and cleaning procedure as we reported earlier.[22,23] Briefly, PMMA was spin-coated on one side of the as-grown graphene on copper foil followed by a copper etch in iron chloride solution (0.1 g mL^{-1}) for 10 h. After removing the Cu foil, the PMMA/graphene was floated on DI water for 12 h, and rinsed with DI water four times. The graphene films in the other group (Group B) were treated additionally with acids and bases after removing the Cu foil by floating the PMMA/

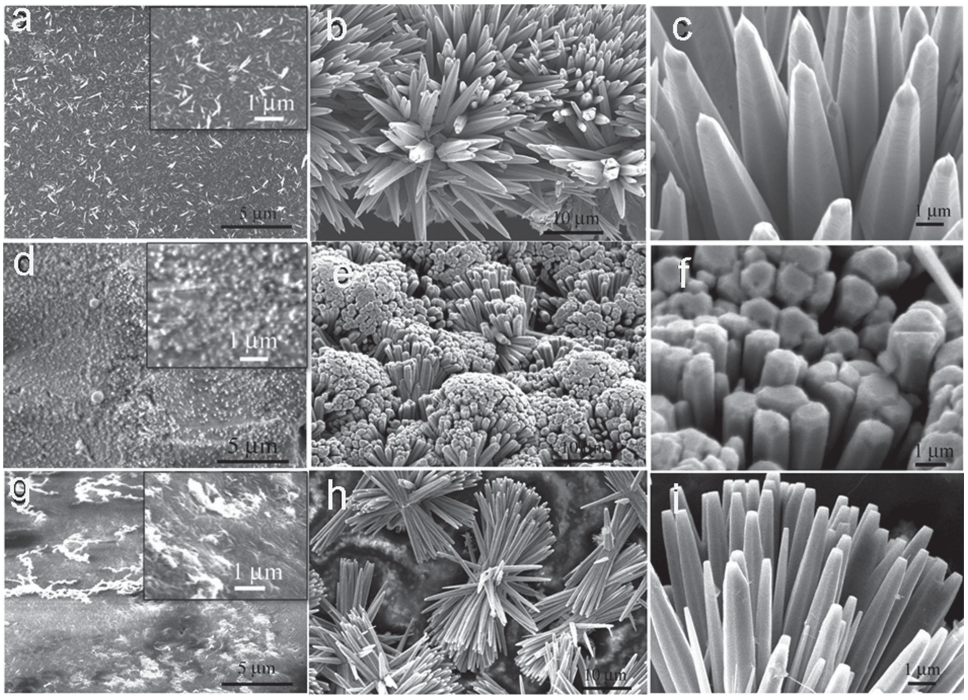

Figure 2. a) SEM images of the ZnO on graphene with growth time of b) 3 and c) 12 h in the face-down floating configuration. The graphene film was treated with a standard transfer and cleaning procedure as detailed in the experiment session before ZnO growth (Group A); d) SEM images of the ZnO on graphene with growth time of e) 3 and f) 12 h in the face-down floating configuration. The graphene film was treated with additional steps of cleaning using diluted HCl (0.1 M) and diluted NaOH (0.1 M) (Group B); g) SEM images of the ZnO on graphene with growth time of e) 3, and f) 12 h in the face-up in solution configuration (Group C). The graphene surface cleaning is the same as for Group A.

graphene films in diluted HCl (0.1 M) for 1 h and diluted NaOH (0.1 M) for 1 h. This acid and base treatment can remove the Cu catalyst residues more thoroughly. In particular, the single-layer CVD graphene was found intact after this additional graphene cleaning procedure. Group C graphene samples were treated with the same transfer and cleaning procedure as was Group A, but the ZnO growth was in the face-up configuration.

Figure 2 compares the sample morphology using scanning electron microscopy (SEM) on representative ZnO/graphene nanohybrid samples from the three groups grown in solution for 3 and 12 h. ZnO was found to uniformly nucleate on graphene films in the face-down floating configuration (Groups A and B), while differences can be observed in their initial nucleation patterns due to the different graphene surface preparations. On Group A samples, a dense, uniform layer of ZnO crystalline nanorods was formed on the graphene surface after 3 h of ZnO growth (Figure 2a). The diameter of the ZnO nanorods is in the range of several to several tens of nanometers, and most nanorods are not perpendicular to the graphene. On Group B samples with the same growth time, a layer of uniform but much denser and smaller ZnO nanoparticles or short nanorods was observed instead with diameters of 5 to 20 nm. In particular, these nanorods are predominantly along the normal direction of the graphene. The difference in the ZnO nucleation layer morphology between Groups A and B suggests graphene surface cleaning plays a critical role, and the additional acid/base cleaning step has indeed promoted the nucleation of ZnO on graphene. In contrast, only sparse ZnO nucleation was observed in Group C after 3 h ZnO growth in solution (Figure 2g). This is not surprising since accumulation of reaction residues on the surface of graphene is clearly seen, which prevents nucleation of ZnO on the graphene surface. Nevertheless, this result confirms that ZnO nucleation can occur directly on clean CVD graphene, which is well known to contain various growth defects[18] which act as nucleation sites for the hydroxyl groups (-OH) available in solution.[19] Furthermore, if the graphene surface is kept clean for an extended period like in the floating face-down configuration, ZnO nucleation directly on graphene can be achieved without a seeding layer at low temperatures below 100 °C in solution.

Increasing the growth time to 12 h, ZnO micro/nanowire arrays can be seen in all three groups of samples (Figure 2b,e,h), but considerable differences remain in the ZnO morphology. In the Group B samples, the ZnO micro/nanowires are predominantly aligned along the normal direction of the graphene, while those in Group C grew horizontally along the graphene surface. The ZnO micro/nanowires in Group A have orientations spreading between vertical and horizontal. The difference in the orientations of the ZnO micro/nanowires may be attributed to the difference in the ZnO nuclei areal densities in the three cases. The highest density of the ZnO micro/nanowires in Group B samples provides the strongest lateral physical confinement in a similar fashion to the case of vertically aligned carbon nanotubes,[24,25] resulting in ZnO micro/nanowire

alignment in the vertical direction (Figure 2e). With less dense ZnO nucleation in Group A, the ZnO micro/nanowires are more spayed around the vertical direction (Figure 2b). This lateral physical confinement is obviously lacking in the face-up configuration due to the low-density ZnO nucleation, leading to ZnO micro/nanowires growing along the surface of graphene. In particular, the coverage of the graphene surface by reaction residues between different ZnO micro/nanowire bundles is evident in Figure 2h. This observation of the correlation between ZnO micro/nanowire orientation and the wire's physical confinement is important for controllable growth of ZnO micro/nanowire arrays on selected areas with desired morphology. Besides the orientations, the densities of ZnO micro/nanowires are considerably different in samples from Groups A, B and C. A higher ZnO micro/nanowires density was observed in the face-down configuration, as shown in Figure 2b,e, as compared to the face-up counterpart shown in Figure 2h. Although a quantitative correlation between ZnO micro/nanowire density and photoresponsivity requires a systematic characterization of the geometry and density of the micro/nanowires, it is generally agreed that a higher density will result in a higher effective thickness of ZnO for the absorption of incident photons. This translates to higher photocurrent of the UV detectors based on the vertically aligned ZnO micro/nanowires on graphene. In addition, the vertical alignment of the ZnO micro/nanowires provides the shortest pathway for photo-charge transport compared to other alignments. Therefore, the face-down growth configuration is more favorable than the face-up configuration for high-performance UV detectors.

A closer look of the ZnO micro/nanowires in Group A (Figure 2c) shows that the wires have pencil-like tips with highly non-uniform stem diameters ranging from 0.1–3 μm and tip diameters of a few hundred nanometers. The length of the ZnO micro/nanowires is in the range of 15–20 μm after 12 h of growth. In the Group B samples (Figure 2e), the ZnO micro/nanowires have flat tips with more uniform stem diameters in the range of 500–1500 nm. The length of the ZnO micro/nanowires in Group B is comparable to that of the Group A samples after 12 h of growth, suggesting a comparable growth rate along the wire axial direction. In the Group C samples (Figure 2i), ZnO micro/nanowires have similar morphology to those in Group A except they have smaller stem diameters ranging from 300–1000 nm. Since the wire lengths are comparable in all three groups, the ZnO axial growth rate seems independent of the sample configuration in solution. The ZnO micro/nanowires all have hexagonal cross sections, which is anticipated for c-axis oriented growth[26] because of the highest-energy of the low-index surfaces of ZnO [0001].[27,28] It is however unclear what determines the lateral growth rate of the ZnO micro/nanowires. A possible limiting factor of the growth rate may relate to the local availability of reactants. In Group A, the stem of the ZnO micro/nanowires are spread out, giving easier access to the reactants and therefore a higher lateral growth rate. This is in contrast to a much tighter spacing between more parallel ZnO micro/nanowires in Groups B and C, which may results in smaller stem diameters due to the lower lateral growth rate. This may also explain the observed difference in the tip shape between ZnO micro/nanowires in Group A (pencil-like) and in Groups B and C (flat top). The more or less equal availability of the reactants around the ZnO micro/nanowires in the former case may lead to more rounded growth, although anisotropic in axial and radial directions, over the wire. In the former case, the nearly homogenous concentration of reactants could lead to more grounded growth of each micro/nanowire, though this also produces anisotropy across the micro/nanowire bundle, both axially and radially. In the later case, especially in Group B, there is an anisotropic density of reactants around the wire caused by their promimity, producing preferential growth at the tip along the energetically preferred ZnO [0001] direction.

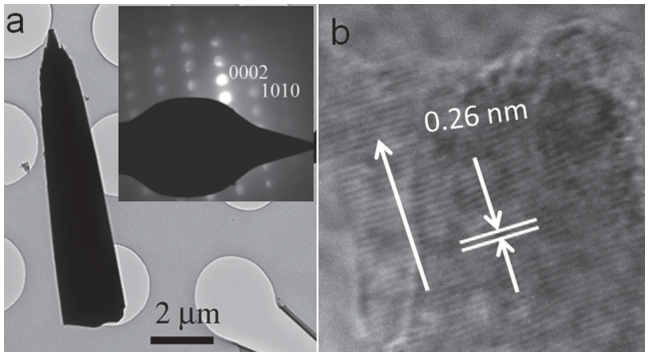

Figure 3. a) TEM image of a ZnO microwire grown in face-down floating configuration. Inset shows a SAED pattern taken on this ZnO microwire; b) HRTEM image of a ZnO wire revealing the ZnO [0001] fringes perpendicular to the wire axis on average separated by 0.26 nm, indicating the crystalline ZnO growth along the ZnO [0001] direction.

A further investigation on the ZnO micro/nanowire structure using transmission electron microscopy (TEM) reveals that the ZnO micro/nanowires from all three groups are single crystalline wurtzite hexagonal phase. **Figure 3**a shows a low magnification TEM image of a representative ZnO microwire grown in the face-down configuration for 12 h (Group A). High-resolution TEM (HRTEM) (Figure 3b) revealed ZnO [0001] fringes perpendicular to the wire axis separated by 0.26 nm on average, indicating crystalline ZnO growth along the ZnO [0001] direction. This is consistent with the selected area electron diffraction (SAED) pattern taken on the ZnO wire (inset of Figure 3a), exhibiting single crystal structure with axial orientation along [0001] direction.

Figure 4a shows a representative Raman spectrum of the original CVD graphene used in this work. Two peaks are clearly seen. The G peak at around 1580 cm^{-1} is due to the doubly degenerate zone center E_{2g} mode, corresponding to in-plane carbon-atom stretching vibrations.[29] The 2D peak at around 2700 cm^{-1} is attributed to the second order zone-boundary phonons.[30] The intensity ratio of the 2D and G peaks is typically above 2. This, together with symmetry of the G and 2D peaks, confirms the CVD graphene is single layer.[31] The D peak at ≈1350 cm^{-1}, due to the breathing modes of sp^2 rings and the active phonons being excited in defective graphene,[32] is barely observable, suggesting the high quality of the graphene used in this work. Similar Raman spectra were observed on graphene samples in Groups A and B, indicating the additional acid+base treatment was benign to graphene. The inset of Figure 4a shows the Raman spectrum taken on a Group B

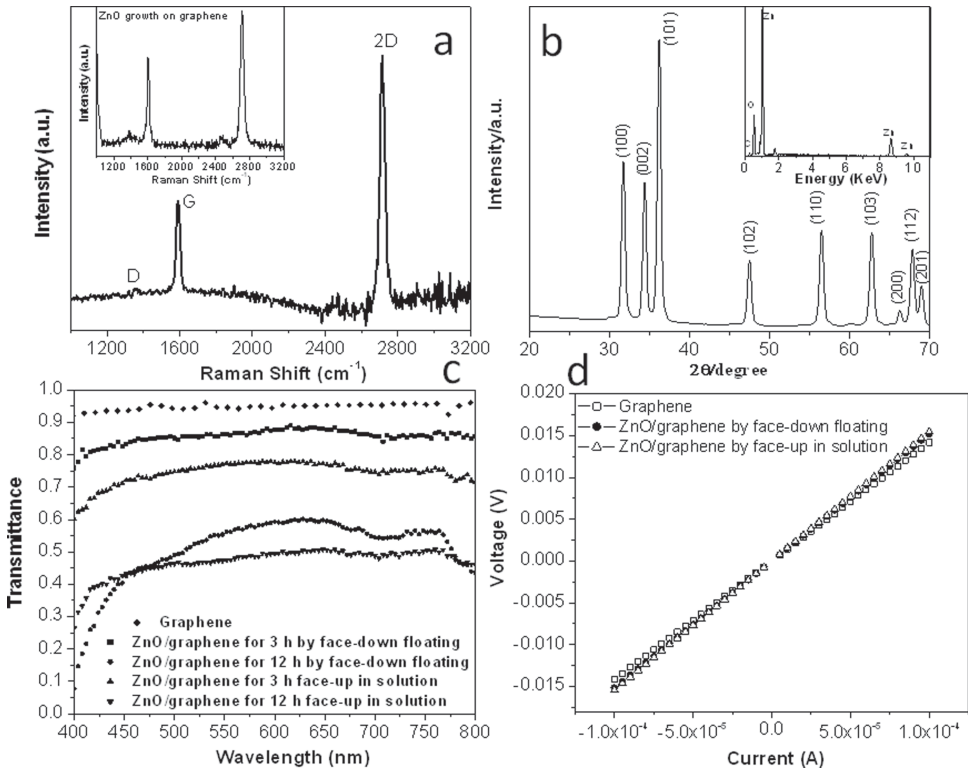

Figure 4. a) Raman spectra of an original CVD graphene and a sample from Group B after ZnO growth for 3 h (inset); b) XRD pattern and EDS (inset) of a ZnO micro/nanowires sample from Group A with 12 h ZnO growth time; c) Optical transmission spectra of an original graphene together with two ZnO/graphene hybrid samples grown for 3 and 12 h, respectively, in face-up in solution configuration (Group C) and face-down floating configuration (Group A); d) *I–V* curves of an original CVD graphene and ZnO/graphene hybrids grown in face-down floating process and face-up in solution, respectively.

sample after ZnO growth in solution for 3 h. The intensity of the D peak increases slightly while the G and 2D peaks are more or less the same as in the original graphene before ZnO growth, suggesting the graphene remained intact after ZnO growth in solution. The slightly increased D peak intensity may be attributed to the attachment of ZnO on graphene. The peak at around 1000 cm^{-1} can be assigned to the OCH_3 rock vibration interacting with the stretch vibrations of the COC group from the PMMA supporting graphene. After 12 h of growth of ZnO on graphene, X-ray diffraction (XRD) was used to analyze the crystal structure of the ZnO micro/nanowires and the result is depicted in Figure 4b. The XRD θ–2θ pattern of a representative sample from Group A after 12 h of growth reveals a set of diffraction peaks indexed to a wurtzite ZnO structure (JCPDS card no. 36-1451) and the lattice constants of this hexagonal phase are c_0 = 5.21 Å and a_0 = 3.25 Å.[33] This is consistent with the HRTEM result. The XRD peaks of (100), (002) and (101) are the most intense. While the (002) peak is expected for c-axis oriented ZnO micro/nanowires, the (100) and (101) peaks are also anticipated from the tilted ZnO micro/nanowires. The chemical composition of ZnO rods on graphene was analyzed using energy dispersive X-ray spectroscopy (EDS), as shown in the inset of Figure 3b, with confirmation of Zn and O, and C from ZnO/graphene hybrid structures.

The optical transmittance and electrical conductivity of the ZnO/graphene play a critical role in utilizing such a hybrid structure in optoelectronic devices. Figure 4c shows the transmittance spectra of the samples of ZnO grown on graphene for 3 and 12 h in face-down (Group A) and face-up (Group C) configurations with respect to the original graphene as a reference. For Group A, ZnO/graphene sample after 3 h of ZnO growth shows rather high transmittance over the visible spectrum with relatively flat transmittances ranging from 80% to 86%. This is in contrast to lower transmittance ranging from 70% to 75% in the Group C sample of the same growth time, possibly due to accumulation of reaction residues on the sample. As the growth time increases to 12 h, the transmittances of both types of samples decrease considerably, especially at the shorter wavelengths towards the UV range. This is anticipated from the UV absorption of the ZnO. It should be noted that the band gap of ZnO is 3.37 eV, which is in the UV range.[34] At a wavelength of 400 nm (the lower limit of the instrument), the transmittance is below 10% for the Group A samples, which is considerably lower than that of 30% for the Group C samples, probably due to the much denser array of ZnO micro/nanowires in the former. On the other hand, the absorption of visible light, which increases with ZnO growth time in Group A samples (or the effective ZnO layer thickness), may be attributed to the presence of oxygen vacancies in the ZnO.[35,36] Although post annealing in oxygen may reduce the oxygen vacancies in ZnO, no annealing was made to the ZnO/graphene hybrid structures in this work to minimize possible oxidation of graphene. It is worth noting

that the electrical conductivity of the graphene remained nearly unchanged after the ZnO growth. Figure 4d compares the *I–V* curves for the original graphene and graphene with ZnO micro/nanowires grown in the face-down (Group A) and face-up (Group C) configurations for 12 h. The electrical conductivity for the ZnO/graphene hybrid samples decreased by 7–9% as compared to that of the original graphene. This may be attributed to the additional charge scattering from the ZnO/graphene interfaces after ZnO attachment, which seems to be consistent with the increase of the D peak amplitude (defects) observed in the Raman spectra on graphene after ZnO growth. Nevertheless, the minor decrease of the conductivity suggests the graphene remains intact during ZnO solution growth. This is likely due to a lower growth temperature, compared to other procedures, and the elimination of a ZnO seeding layer which can cause damage to the graphene surface.

The ZnO/graphene nanohybrids are excellent candidates for various applications in photodetection and gas sensing. In particular, the vertically aligned 3D single-crystalline ZnO micro/nanowire arrays on graphene offer increased surface area and effective thickness compared to the 2D thin films. Both are critical to the sensitivity of the detectors and sensors. Furthermore, direct growth of the ZnO nanostructures on graphene may allow a better ZnO/graphene interface, facilitating charge transport and thus improved responsivity and response time. According to the first principles calculations based on density functional theory, ZnO formed a strong and stable bond and adhere on graphene.[37] As a proof of concept, UV detectors were fabricated using the ZnO micro/nanowires on CVD graphene, with the graphene acting as one electrode and fluorine doped tin-oxide (FTO) used as the other. This is depicted schematically in **Figure 5**a. Slight pressure was applied to ensure the contact between the ZnO micro/nanowires and the FTO electrode. Figure 5b shows the energy level diagram of the graphene with a work function of 4.6 eV,[38] FTO at 4.9 eV, and ZnO with the conduction band edge of 4.2 eV and valance band edge of 7.6 eV.[39] The barrier between the graphene Fermi energy and ZnO conduction band edge is -0.4 eV, which is favorable for photoelectron injection from ZnO to graphene. The ZnO/FTO band-edge offset is +2.7 eV, allowing hole injection to FTO. Figure 5c compares the *I–V* curves taken from the ZnO/graphene nanohybrid UV detectors in dark and at three different UV light intensities (Varian, Model PS301-1). Upon UV illumination, a considerable increase in photoconductivity can be clearly seen,[40] suggesting a well formed interface between ZnO and graphene for photocarrier transport. With increasing intensity of UV light in the range of 18 mW cm^{-2} to 22 mW cm^{-2} (instrumentation limit), a monotonic increase of the photocurrent was observed. The inset of Figure 5c plots the UV photoresponsivity (black curve) and responsivity per voltage (red curve) against the bias voltage applied between the graphene anode and FTO cathode. Both curves follow a linearly increasing trend at lower bias below ≈6 V followed by a slightly accelerated increase at higher bias up to 8.5 V. It should be mentioned that low bias is preferred for detector operation. At 8.5 V bias, the photocurrent is 6.3×10^{-4} A at the UV light intensity of 18 mW cm^{-2}, which yields the photoresponsivity around 13.8 A W^{-1} or 1.62 A W^{-1} per volt for the ZnO/graphene nanohybrid UV detectors. This is a 500% increase over the photoresponse of 0.3 A W^{-1} per volt on epitaxial ZnO thin film Schottky UV detectors[41] and a 300% increase over that of the ZnO nanoparticle film detectors[42] due to larger surface area and effective thickness of our 3D ZnO nanostructures. In addition, the responsivity obtained in this work is about 56% over that of reported ZnO nanowires photodetectors,[43] and 40% higher than the best previous report of 22.7 A W^{-1} at 20 V bias (or 1.14 A W^{-1} per volt) on UV detectors consisting of randomly oriented ZnO nanorods on graphene flakes.[10]

A much shorter photoresponse time was observed in the vertically aligned ZnO micro/nanowires on CVD graphene nanohybrids fabricated in the seedless floating process developed in this work. As illustrated in Figure 5d, the photocurrent responds to the "on" and "off" of the UV light almost instantaneously. The detector response time, defined as the time for the current to rise from 10% to 90% of saturation value (point A to

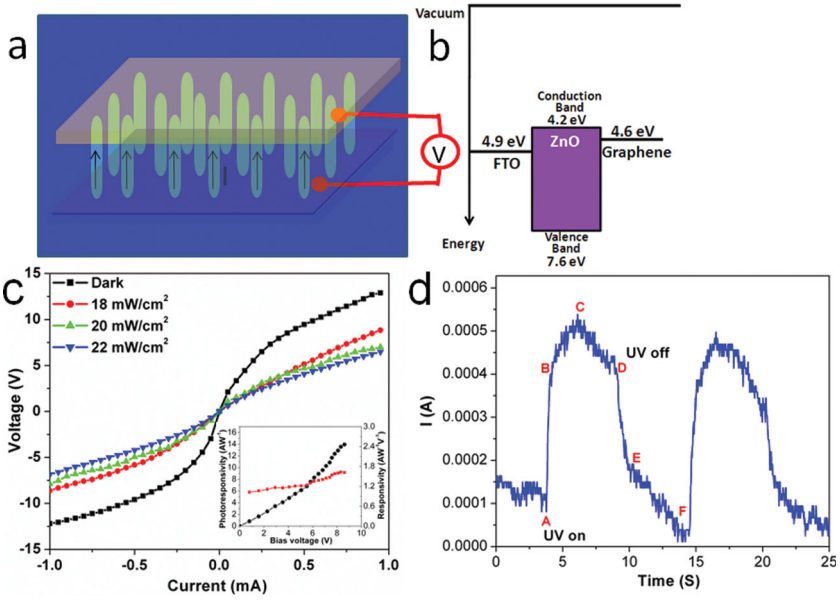

Figure 5. a) A schematic description of the vertically aligned ZnO micro/nanowire/graphene hybrid UV detector with graphene anode (bottom) and FTO cathode (top). b) Energy diagram for the device with work function values for the FTO and graphene, and conduction and valence band edges for ZnO labelled. c) *I–V* characteristic curves of the ZnO/graphene hybrid UV detectors in the dark (black curve) and with UV illumination at 18 mW cm^{-2} (red curve), at 20 mW cm^{-2} (green curve), at 22 mW cm^{-2} (blue curve), respectively. Inset shows the photoresponsivity (black curve), photoresponsivity/voltage (red curve) vs. bias voltage at the UV light intensity of 18 mW cm^{-2}. d) Temporal photoresponse of the ZnO/graphene hybrid UV detectors to UV light ON-OFF cycles with: A-UV on, B-90% of the photocurrent saturation value, C- the photocurrent saturation value, D-UV off, E-the shift point of from quick drop to slow decay, and F-background current immediately before UV light was on again.

B), is 0.3 s. In addition, some undesirable features are clearly seen in the dynamic photoresponse. For example, the top part of the photoresponse (from B to C and then to D) is rounded instead of square, suggesting a slower process co-exists with the faster UV response. When turning off the UV light at point D, the photocurrent quickly drops (point D to E) in about 2.5 seconds, but this is followed with a slower decay (E to F) in 4 seconds. The asymmetric faster rise and slower fall times of the photocurrent in response to the UV light "on" and "off" suggest charge traps in ZnO, This is a well known effect due to the existence of defects such as oxygen vacancies, oxygen absorption/desorption on ZnO surfaces, grain boundaries, imperfections in crystallinity, etc.[44] On epitaxial ZnO film Schottky UV detectors, which probably have a minimum number of these traps, a rise time of 12 ns and fall time of 50 ns were observed.[41] In constrast, UV detectors based on polycrystalline ZnO films, which can be made at a much lower cost as compared to the epitaxial counterparts, suffer significant charge trapping with response time ranging from minutes to h.[45,46] This suggests the ZnO crystallinity plays a critical role in determining the response time and explains the improved response time on single-crystalline ZnO nanowire UV detectors with reported rise times of 0.7–1 s and fall times up to 3 s.[47,48] The comparable response time (rise time of ≈0.3 s and fall time of 2.5 s) obtained in this work suggests high-quality crystallinity can be achieved in vertically aligned ZnO micro/nanowires grown directly on graphene using the seedless floating growth process in solution. It is particularly worth noting that the detector response time achieved in this work is three orders of magnitude faster than that of the previously reported ZnO nanowires/graphene hybrids, indicating the obtained ZnO/graphene hybrids are high-quality crystalline ZnO with a clean graphene interface, both are keys to reducing charge traps and facilitating charge transport.[10]

3. Conclusions

In conclusion, a novel seedless floating growth process in solution has been developed for the growth of crystalline ZnO micro/nanowire arrays on single-layer graphene sheets made by CVD. The ZnO micro/nanowire arrays' alignment was controlled by the physical confinement; increasing this confinement changed the alignment from horizontal (parallel to graphene) to vertical (perpendicular to graphene). In particular, vertically aligned ZnO micro/nanowire arrays were obtained on graphene by employing a face-down floating configuration plus a graphene surface cleaning treatment to promote high-density ZnO nucleation on graphene. These 3D ZnO/graphene hybrid nanostructures provide an ideal template for UV detectors due to the superior wavelength selectivity and charge mobility. The obtained high responsivity of 1.62 A W^{-1} per volt represents about 500% improvement over that of the conventional epitaxial ZnO thin film UV detectors, 300% over the ZnO nanoparticle film photodetector, and at least 40% over the best results reported previously on ZnO nanowires/graphene hybrid and other ZnO nanostructure UV detectors. It is particularly worth noting that the detector response time achieved in this work is three orders of magnitude faster than that of the previously reported ZnO nanowires/graphene hybrids and comparable to the best reported on UV detectors made of high-quality single-crystalline ZnO nanostructures. Considering this seedless solution process can be carried out in air at a low temperature of around 80 °C, it has a promising potential for low-cost commercialization of ZnO/graphene hybrids at low costs for various applications of photodetectors, photovoltaics, photocatalysis, gas sensors, biosensors, and other optoelectronic devices.

4. Experimental Section

Graphene was grown on commercial copper foils with 25 μm thickness (Alfa Aesar, item No.13382) at ≈1000 °C in a CVD system using a similar pro-cedure to that described elsewhere.[23,49] A mixture of CH_4 (35 sccm) and H_2 (2 sccm) was used as the gas precursors. Poly-methyl methacrylate (PMMA) was spin-coated on one side of the as-grown graphene before the sample was immersed into iron chloride solution (0.1 g mL^{-1}) for removal of the copper foil. After removing the Cu foil, the graphene sheets were cleared with DI water, and either placed face-down or attached to a substrate for face-up in solution configuration $Zn(NO_3)_2$ and ammonia solution (pH > 10) at 60–90 °C for 3–12 h) for growth of ZnO micro/nanowires on graphene. In the former case, since the polymer/graphene composite sample has a lower density than that of the solution, the sample was floating on the surface of the solution during the entire procedure of the ZnO growth with graphene side face down. In the latter case, the graphene/polymer/substrate sample remained in the face-up configuration at the bottom of the solution during the ZnO growth. After the growth, the hybrid ZnO/graphene nanostructures were transferred onto Si or glass substrates for characterization of the physical properties.

The SEM images were taken with Jeol JSM-6380. XRD pattern was obtained by using Bruker SMART APEX with Cu Kα radiation (λ = 1.5405 Å). The TEM and HRTEM images and diffraction patterns were obtained using FEI Tecnai F20 XT Field Emission Transmission Electron Microscope. The transmittance spectra were obtained with iHR 550 instruments. Raman spectra were taken with WITec alpha 300 using laser excitation of 488 nm.

Supporting Information

Supporting Information is available from the Wiley Online Library or from the author.

Acknowledgements

The authors acknowledge support in part by ARO contract No. ARO-W911NF-09–1–0295, W911NF-12-1-0412, and NSF contracts Nos. NSF-DMR-1105986 and NSF EPSCoR-0903806, and matching support from the State of Kansas through Kansas Technology Enterprise Corporation. The authors would like to thank A.J. Elliot and Melisa Xin for their help editing this paper.

Received: February 4, 2013
Revised: March 7, 2013
Published online: April 15, 2013

[1] K. S. Novoselov, A. K. Geim, S. V. Morozov, D. Jiang, M. I. Katsnelson, I. V. Grigorieva, S. V. Dubonos, A. A. Firsov, *Nature* **2005**, *438*, 197.
[2] A. K. Geim, K. S. Novoselov, *Nat. Mater.* **2007**, *6*, 183.
[3] K. S. Novoselov, A. K. Geim, S. V. Morozov, D. Jiang, Y. Zhang, S. V. Dubonos, I. V. Grigorieva, A. A. Firsov, *Science* **2004**, *306*, 666.
[4] J. W. Bai, X. Zhong, S. Jiang, Y. Huang, X. F. Duan, *Nat. Nanotechnol.* **2010**, *5*, 190.
[5] M. Y. Han, B. Ozyilmaz, Y. B. Zhang, P. Kim, *Phys. Rev. Lett.* **2007**, *98*, 206805.

[6] K. Todd, H. T. Chou, S. Amasha, D. Goldhaber-Gordon, *Nano. Lett.* **2009**, *9*, 416.
[7] P. V. Kamat, *J. Phys. Chem. Lett.* **2011**, *2*, 242.
[8] Y. Y. Liang, H. L. Wang, H. S. Casalongue, Z. Chen, H. J. Dai, *Nano. Res.* **2010**, *3*, 701.
[9] Z. Y. Chen, S. Berciaud, C. Nuckolls, T. F. Heinz, L. E. Brus, *ACS Nano* **2010**, *4*, 2964.
[10] H. X. Chang, Z. H. Sun, K. Y. F. Ho, X. M. Tao, F. Yan, W. M. Kwok, Z. J. Zheng, *Nanoscale* **2011**, *3*, 258.
[11] S. O. Kim, J. O. Hwang, D. H. Lee, J. Y. Kim, T. H. Han, B. H. Kim, M. Park, K. No, *J. Mater. Chem.* **2011**, *21*, 3432.
[12] K. Chung, C. H. Lee, G. C. Yi, *Science* **2010**, *330*, 655.
[13] S. W. Hwang, D. H. Shin, C. O. Kim, S. H. Hong, M. C. Kim, J. Kim, K. Y. Lim, S. Kim, S. H. Choi, K. J. Ahn, G. Kim, S. H. Sim, B. H. Hong, *Phys. Rev. Lett.* **2010**, *105*, 127403.
[14] B. Kumar, K. Y. Lee, H. K. Park, S. J. Chae, Y. H. Lee, S. W. Kim, *ACS Nano* **2011**, *5*, 4197.
[15] D. Choi, M. Y. Choi, W. M. Choi, H. J. Shin, H. K. Park, J. S. Seo, J. Park, S. M. Yoon, S. J. Chae, Y. H. Lee, J. Y. Choi, S. Y. Lee, J. M. Kim, S. W. Kim, *Adv. Mater.* **2010**, *22*, 2187.
[16] J. A. Lin, M. Penchev, G. P. Wang, R. K. Paul, J. B. Zhong, X. Y. Jing, M. Ozkan, C. S. Ozkan, *Small* **2010**, *6*, 2448.
[17] W. I. Park, J. M. Lee, Y. B. Pyun, J. Yi, J. W. Choung, *J. Phys. Chem. C* **2009**, *113*, 19134.
[18] Y. F. Zhang, T. Gao, Y. B. Gao, S. B. Xie, Q. Q. Ji, K. Yan, H. L. Peng, Z. F. Liu, *ACS Nano* **2011**, *5*, 4014.
[19] F. B. Banhart, F. J. Kotakoski, A. V. Krasheninnikov, *ACS Nano* **2011**, *5*, 26.
[20] R. Viswanatha, P. K. Santra, C. Dasgupta, D. D. Sarma, *Phys. Rev. Lett.* **2007**, *98*, 255501.
[21] H. Wang, J. A. Xie, K. P. Yan, M. Duan, *J. Mater. Sci. Technol.* **2011**, *27*, 153.
[22] J. W. Liu, J. Wu, C. M. Edwards, C. L. Berrie, D. Moore, Z. J. Chen, V. A. Maroni, M. P. Paranthaman, A. Goyal, *Adv. Funct. Mater.* **2011**, *21*, 3868.
[23] J. W. Liu, G. W. Xu, C. Rochford, R. T. Lu, J. Wu, C. M. Edwards, C. L. Berrie, Z. J. Chen, V. A. Maroni, *Appl. Phys. Lett.* **2011**, *99*, 023111.
[24] J. W. Liu, X. J. Li, A. Schrand, T. Ohashi, L. M. Dai, *Chem. Mater.* **2005**, *17*, 6599.
[25] R. Andrews, D. Jacques, A. M. Rao, F. Derbyshire, D. Qian, X. Fan, E. C. Dickey, J. Chen, *Chem. Phys. Lett.* **1999**, *303*, 467.
[26] L. E. Greene, M. Law, J. Goldberger, F. Kim, J. C. Johnson, Y. F. Zhang, R. J. Saykally, P. D. Yang, *Angew. Chem. Int. Ed.* **2003**, *42*, 3031.
[27] N. L. Allan, F. Claeyssens, C. L. Freeman, Y. Sun, M. N. R. Ashfold, J. H. Harding, *J. Mater. Chem.* **2005**, *15*, 139.
[28] L. E. Greene, M. Law, D. H. Tan, M. Montano, J. Goldberger, G. Somorjai, P. D. Yang, *Nano Lett.* **2005**, *5*, 1231.
[29] Y. F. Hao, Y. Y. Wang, L. Wang, Z. H. Ni, Z. Q. Wang, R. Wang, C. K. Koo, Z. X. Shen, J. T. L. Thong, *Small* **2010**, *6*, 195.
[30] A. C. Ferrari, J. C. Meyer, V. Scardaci, C. Casiraghi, M. Lazzeri, F. Mauri, S. Piscanec, D. Jiang, K. S. Novoselov, S. Roth, A. K. Geim, *Phys. Rev. Lett.* **2006**, *97*, 187401.
[31] X. S. Li, Y. W. Zhu, W. W. Cai, M. Borysiak, B. Y. Han, D. Chen, R. D. Piner, L. Colombo, R. S. Ruoff, *Nano Lett.* **2009**, *9*, 4359.
[32] A. C. Ferrari, *Solid State Commun.* **2007**, *143*, 47.
[33] B. Liu, H. C. Zeng, *J. Am. Chem. Soc.* **2003**, *125*, 4430.
[34] X. D. Wang, C. J. Summers, Z. L. Wang, *Nano Lett.* **2004**, *4*, 423.
[35] S. Baruah, S. S. Sinha, B. Ghosh, S. K. Pal, A. K. Raychaudhuri, J. Dutta, *J. Appl. Phys.* **2009**, *105*, 074308.
[36] R. M. Sheetz, I. Ponomareva, E. Richter, A. N. Andriotis, M. Menon, *Phys. Rev. B* **2009**, *80*, 195314.
[37] W. M. Choi, K. S. Shin, H. S. Lee, D. Choi, K. Kim, H. J. Shin, S. M. Yoon, J. Y. Choi, S. W. Kim, *Nano Res.* **2011**, *4*, 440.
[38] P. Kim, Y. J. Yu, Y. Zhao, S. Ryu, L. E. Brus, K. S. Kim, *Nano Lett.* **2009**, *9*, 3430.
[39] R. Konenkamp, R. C. Word, M. Godinez, *Nano Lett.* **2005**, *5*, 2005.
[40] J. W. Liu, X. J. Li, L. M. Dai, *Adv. Mater.* **2006**, *18*, 1740.
[41] S. Liang, H. Sheng, Y. Liu, Z. Huo, Y. Lu, H. Shen, *J. Cryst. Growth* **2001**, *225*, 110.
[42] Y. Z. Jin, J. P. Wang, B. Q. Sun, J. C. Blakesley, N. C. Greenham, *Nano Lett.* **2008**, *8*, 1649.
[43] S. Bai, W. W. Wu, Y. Qin, N. Y. Cui, D. J. Bayerl, X. D. Wang, *Adv. Funct. Mater.* **2011**, *21*, 4464.
[44] D. Wang, C. Soci, A. Zhang, B. Xiang, S. A. Dayeh, D. P. R. Aplin, J. Park, X. Y. Bao, Y. H. Lo, *Nano Lett.* **2007**, *7*, 1003.
[45] D. Basak, G. Amin, B. Mallik, G. K. Paul, S. K. Sen, *J. Cryst. Growth* **2003**, *256*, 73.
[46] P. Sharma, K. Sreenivas, K. V. Rao, *J. Appl. Phys.* **2003**, *93*, 3963.
[47] S. N. Das, K. J. Moon, J. P. Kar, J. H. Choi, J. Xiong, T. I. Lee, J. M. Myoung, *Appl. Phys. Lett.* **2010**, *97*, 022103.
[48] X. W. Fu, Z. M. Liao, Y. B. Zhou, H. C. Wu, Y. Q. Bie, J. Xu, D. P. Yu, *Appl. Phys. Lett.* **2012**, *100*, 223114.
[49] X. S. Li, W. W. Cai, J. H. An, S. Kim, J. Nah, D. X. Yang, R. Piner, A. Velamakanni, I. Jung, E. Tutuc, S. K. Banerjee, L. Colombo, R. S. Ruoff, *Science* **2009**, *324*, 1312.